THE ASTROPHYSICAL JOURNAL, 277:865–873, 1984 February 15

INTERPRETATION OF MICROWAVE ACTIVE REGION STRUCTURES USING *SMM* SOFT X-RAY OBSERVATIONS

K. T. STRONG
Space Astronomy Group, Lockheed Missiles and Space Company, Palo Alto, California
C. E. ALISSANDRAKIS
Laboratory of Astrophysics, University of Athens
AND
M. R. KUNDU
Astronomy Program, University of Maryland
Received 1983 February 22; accepted 1983 August 1

ABSTRACT

Microwave ring structures associated with active region sunspots were discovered by Alissandrakis and Kundu; however, there has been some uncertainty as to their origin. In this study, we present combined soft X-ray and microwave data of two active regions, one of which had microwave ring structure. The regions were observed simultaneously by the X-ray Polychromator on the *Solar Maximum Mission* satellite and the Westerbork Synthesis Radio Telescope at 6.16 cm while they were near to disk center on 1980 May 25 and 26. The X-ray spectroheliograms were used to derive the electron temperature and density of the coronal material of the ring structure. No significant variations were found across these regions, so they are not a result of systematic variations in electron temperature and density in the coronal material above sunspots. Model computations are presented which show that the microwave emission at the center of the ring comes from a cooler region.

In the course of this analysis, a cool, compact soft X-ray feature was observed to be associated with one of the main spots. It also corresponded to a microwave and Hα feature. It persisted for at least a day with a high density (10^{11} cm^{-3}) but a low temperature (1.5×10^6 K). To our knowledge, this type of source has not been observed before. Also, the soft X-ray loop arcades were investigated; we find that, although the electron temperature from the X-ray data is comparable to the microwave brightness temperature, the density is too low (6×10^9 cm^{-3}) to account for the emission by the free-free process.

Subject headings: Sun: flares — Sun: radio radiation — Sun: X-rays

I. INTRODUCTION

Alissandrakis and Kundu (1982) reported the detection of a new kind of sunspot-associated microwave source in which the emission in total intensity came predominantly from a ring structure with a size between that of the umbra and the penumbra. They proposed that the newly discovered ring structure could be the product of the low gyroresonance opacity when the angle between the magnetic field and the line of sight is close to zero. Such a structure should exist above the center of a sunspot located near the disk center so that the magnetic field orientation will be predominantly longitudinal. Since, under the conditions (N_e, T_e) prevailing above sunspots, the region of low opacity is very small for the second harmonic and more extended for the third, one expects a decrease in total intensity in such regions. However, the region of low intensity should shift toward the disk center with respect to the region of most intense microwave emission as the source moves toward the limb, contrary to the observations of Alissandrakis and Kundu. It was therefore concluded that in addition to the angle effect, there must be a temperature decrease above the umbra at the level of formation of 6 cm radiation. Indeed, from high-resolution ($\sim 1''$) observations using the VLA, Kundu and Velusamy (1980) and Kundu, Schmahl, and Rao (1981) demonstrated the lack of correlation between the umbra and strong 6 cm emission, and they attributed this to the existence of cool material, similar to that observed in extreme-ultraviolet and X-rays (Foukal *et al.* 1974; Webb and Zirin 1981).

The purpose of this paper is to investigate the roles played by the geometrical effect of gyroresonance absorption and by the low-temperature ($< 10^6$ K) flux tubes above the relevant sunspot, by combining the Westerbork Synthesis Radio Telescope (WSRT) 6 cm observations with the X-ray observations made with the X-ray Polychromator (XRP) on the *Solar Maximum Mission* (*SMM*) satellite. Some features associated with Hale regions 16863 and 16864 (Boulder nos. 2469 and 2470) are analyzed from observations on 1980 May 25 and 26 combined with model computations of the radio emission. The nature of a cool and compact coronal feature seen in soft X-rays, which corresponded to some interesting microwave and magnetic features, is also examined. Finally, we considered the origin of the X-ray and radio emission associated with neutral lines of the magnetic field.

II. OBSERVATIONS AND RESULTS

a) X-Ray Observations

The X-ray data were obtained by the XRP experiment on the *SMM* satellite. The XRP consists of two independent

instruments (for details, see Acton *et al.* 1980): the Flat Crystal Spectrometer (FCS), which mapped the regions, and the Bent Crystal Spectrometer (BCS), which monitored them for flaring activity. The FCS produced simultaneous spectroheliograms in six prominent soft X-ray lines (O VIII, Ne IX, Mg XI, Si XIII, S XV, and Fe XXV) by rastering its 14″ (FWHM) collimated field of view over a 5 arcmin^2 area of the active regions with 15″ pixel spacing. A white-light map was also produced, making it possible to align the X-ray image with the radio maps to an accuracy of about 10″. The FCS data were used to derive the electron temperature and emission measure of various features in the active regions and, hence, to calculate the optical depth of the plasma to microwave radiation.

The FCS observed the active regions, Hale 16863 and 16864, regularly from 1980 May 22 to June 2. However, the observations discussed here are limited to the survey orbits that occurred between 14:10 UT and 14:50 UT on both 1980 May 25 and 26 when there were simultaneous microwave observations from WSRT. During these orbits, four complete 5 arcmin^2 maps centered on the neutral line that lay between the regions were obtained with a cadence of 410 s. The BCS Ca XIX channel, which is sensitive to plasma at a temperature of about 10^7 K or higher, showed no measurable activity during the observations, and so the active regions were stable and quiescent. This was confirmed by the FCS spectroheliograms which only showed significant emission in the three softest channels—O VIII, Ne IX, and Mg XI ($T_{max} \approx 3 \times 10^6$ K, 4×10^6 K, and 7×10^6 K respectively). Only upper limits to the fluxes could be obtained in the other FCS channels, but this was sufficient to establish that there was no significant amount of plasma at any higher temperature. Further, each map in the time sequence obtained showed no significant change in the observed count rate after the cosmic-ray background had been subtracted from the images as described by Schmahl *et al.* (1982).

Figure 1 shows the X-ray data for both days. The spectroheliograms were summed and averaged over each orbit to improve the statistical uncertainty on the count rate from each pixel and to correspond more closely to the synthesized radio maps. This is a valid procedure owing to the stability of the active regions discussed above. Figures 1*a* and 1*b* are the Ne IX and Mg XI contour maps for 1980 May 25. Figure 1*c* is the corresponding white-light image. Figures 1*d* and 1*e* are the corresponding X-ray data for 1980 May 26; note the similarity to the previous day's maps. Figure 1*f* shows the five regions used in the subsequent analysis, labeled A–E. A is located slightly east of the large spot of region 16863 over some small spots and pores, while B corresponds to the microwave ring structure shown in Figures 2*a* and 3*a*. C and D are the groups of pixels that are the brightest soft X-ray features in each active region and, presumably, correspond to the main loop arcades that overlie the neutral line in each active region. Note that, as these regions were near the Sun center at the time of observation, there should be little effect from perspective. The area E is the location of a compact bright region that corresponds to a microwave and H feature. The XRP map includes most of the emission from the two active regions. However, as can be seen from Figure 1*d*, the large spot in the latter region is not entirely within the frame.

The active regions were so quiescent that they were only detectable in the three softest X-ray channels (O VIII, Ne IX, and Mg XI). As the O VIII to Ne IX line intensity ratio is insensitive to temperature variations (Acton and Brown 1978) over the temperature range typical of active regions, there was only one temperature diagnostic available, namely the ratio for the Ne IX to Mg XI line intensities. Hence the assumption that the regions were isothermal was formed upon the analysis of the X-ray data. However, this probably is a good assumption as the regions are observed to be stable and unperturbed by any flaring activity throughout the period of the observations. Observations of brighter active regions and even the late decay of a flare (Veck *et al.* 1984) have shown that an isothermal approximation is valid. Further, if the active region coronal plasma were multithermal, then the line ratio would vary as the FCS scanned across the different temperature regions. No such variations were observed except for a single point (E) which is specifically discussed in § IV.

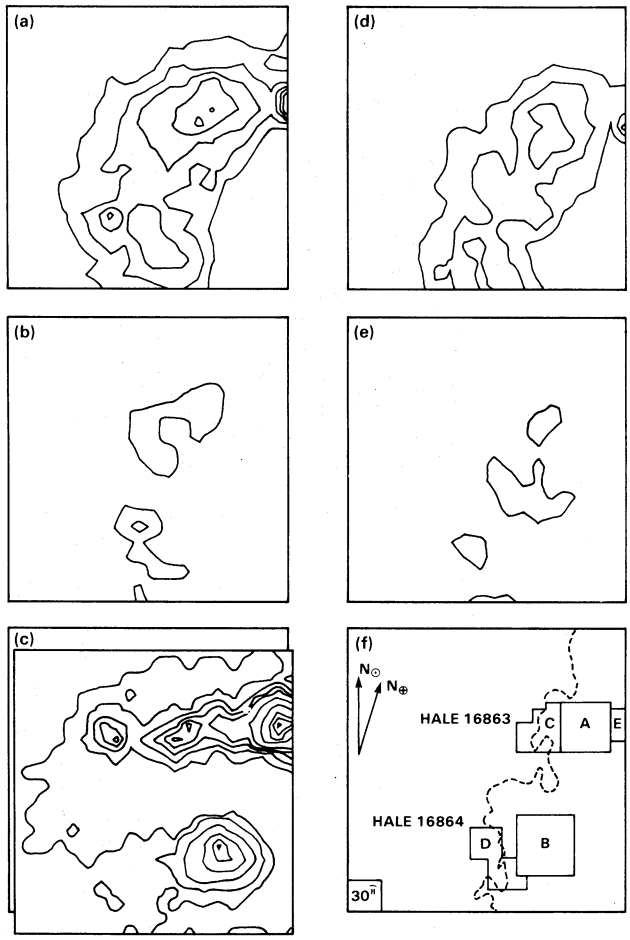

FIG. 1.—FCS maps of Hale regions 16863 and 16864 for 1980 May 25 and 26. The maps are averaged over several samples taken from 14:15 UT to 14:45 UT. The X-ray contour levels represent 15, 30, 45, 60, and 75 counts above background: (*a*) Ne IX for May 25; (*b*) Mg XI for May 25; (*c*) optical sensor showing location of sunspots with respect to the X-ray image on May 25 (note the offset between the X-ray and optical boresights); (*d*) Ne IX for May 26; (*e*) Mg XI for May 26; (*f*) sketch to show locations of the pixel used in the analysis for May 25. The broken line represents the neutral line. A is located east of the main spot of region 16863. B is located above the main spot of 16864 and associated with the 6 cm ring source. C and D are the areas with the brightest X-ray emission. E is a bright, cool X-ray feature associated with the leading spot in Hale 16863.

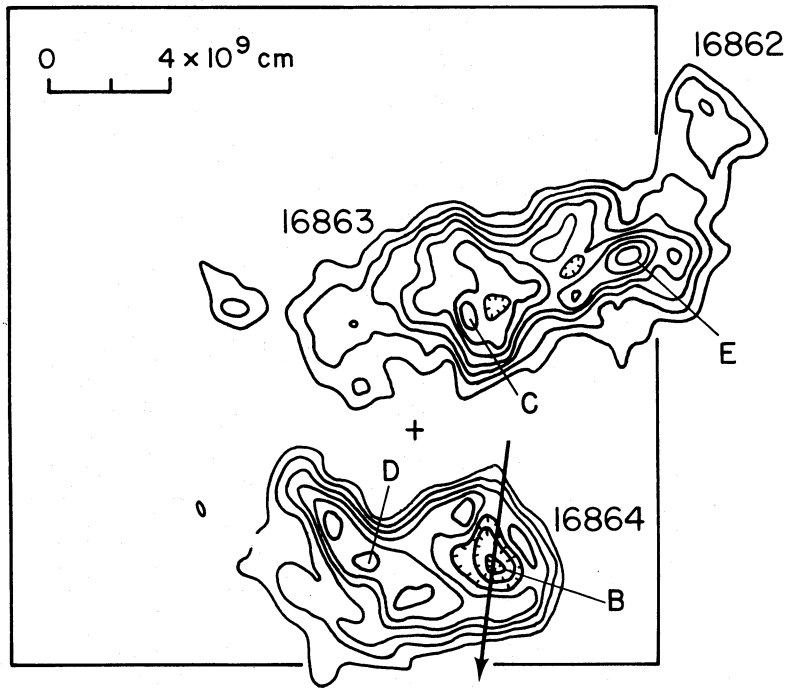

FIG. 2*a*

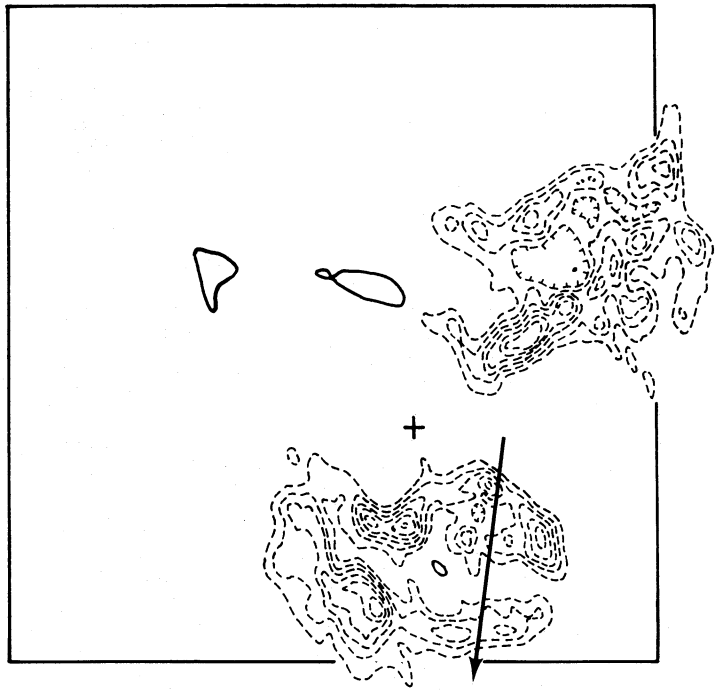

FIG. 2*b*

FIG. 2.—Maps of active regions 16864 and 16863 in (*a*) total intensity and (*b*) circular polarization at 6 cm observed on 1980 May 25. The radio maps also show the trailing part of region 16862. The inner borders correspond to the X-ray field of view shown in Fig. 1, while the plus sign shows the position of the radio fringe stopping center. The radio contours are in steps of 0.48×10^6 K for total intensity and 0.12×10^6 K for circular polarization. Dashed contours indicate left-hand circular polarization, hatched contours indicate decreasing brightness temperature. The arrows indicate the direction of the limb. C and D are the peaks of sources associated with neutral lines and X-ray arcades, and E is the source associated with the bright, cool X-ray feature (see Fig. 1). The angular resolution is 4″ E-W by 12″ N-S (3×10^8 cm by 9×10^8 cm). Solar north is up, solar west to the right.

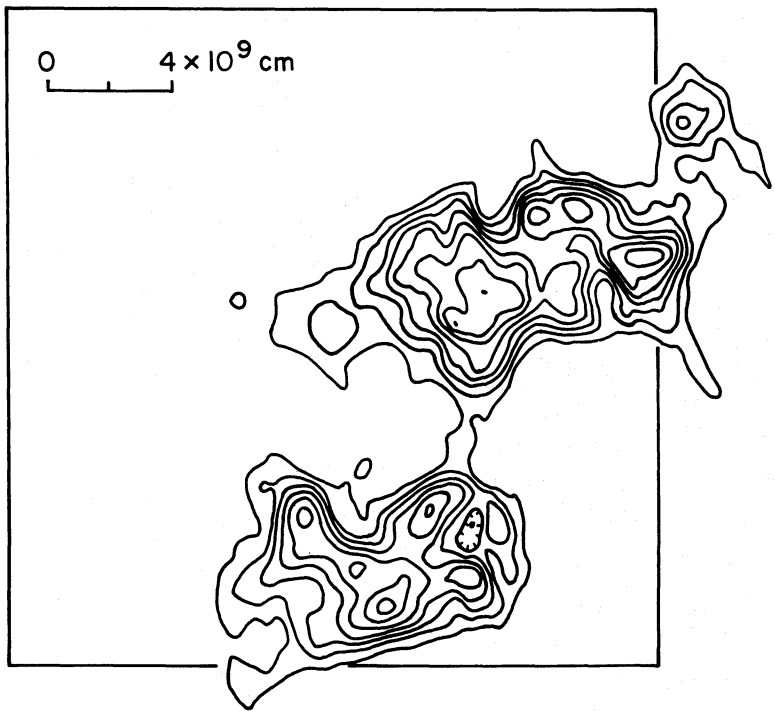

FIG. 3*a*

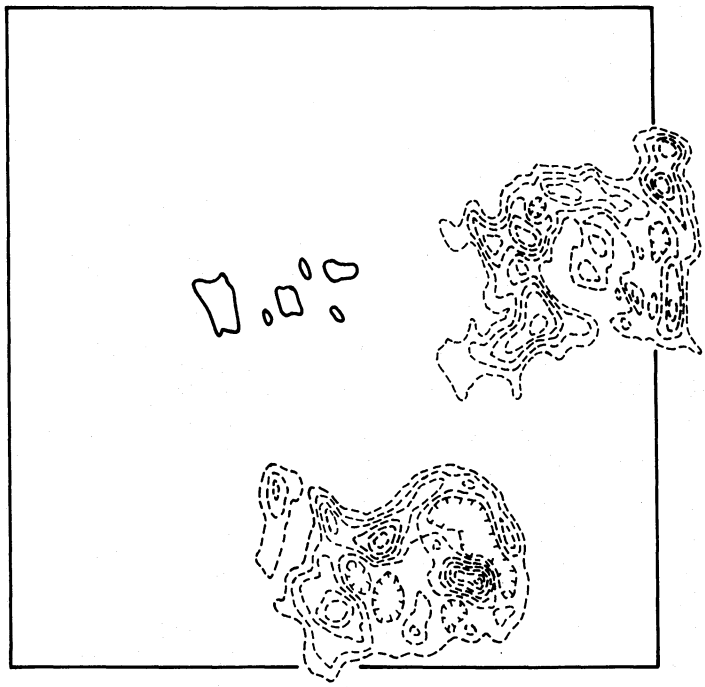

FIG. 3*b*

FIG. 3.—(*a*) and (*b*) Same as Figs. 2*a* and 2*b*, but for 1980 May 26. The radio contours are in steps of 0.4×10^6 K for (*a*) total intensity and 0.11×10^6 K for (*b*) circular polarization.

TABLE 1

X-RAY RESULTS

LOCATION	1980 MAY 25				1980 MAY 26			
	T_e (10^6 K)	N_e[a] (10^9 cm^{-3})	$\tau_{f\text{-}f}$ ($\lambda = 6.16$ cm)	$T_{b,f\text{-}f}$ (10^6 K)	T_e (10^6 K)	N_e[a] (10^9 cm^{-3})	$\tau_{f\text{-}f}$ ($\lambda = 6.16$ cm)	$T_{b,f\text{-}f}$ (10^6 K)
A	2.7(±0.3)	6.5(±1.5)	0.16(±0.11)	0.40(±0.20)	3.0(±0.4)	6.5(±1.5)	0.13(±0.08)	0.38(±0.20)
B:								
Core	2.9(±0.5)	3.6(±1.7)	0.05(±0.05)	0.13(±0.13)	3.3(±0.4)	4.6(±1.6)	0.06(±0.05)	0.19(±0.14)
Halo	2.8(±0.3)	4.6(±1.1)	0.08(±0.05)	0.20(±0.10)	3.2(±0.4)	3.6(±1.3)	0.04(±0.03)	0.12(±0.09)
C	3.0(±0.3)	7.3(±1.7)	0.17(±0.10)	0.47(±0.24)	3.2(±0.3)	5.8(±1.3)	0.10(±0.06)	0.30(±0.15)
D	3.3(±0.4)	4.6(±1.1)	0.06(±0.04)	0.19(±0.10)	3.0(±0.5)	4.6(±1.1)	0.07(±0.05)	0.20(±0.11)
E[b]	1.3(±0.3)	130	189	1.3 (±0.3)	1.2(±0.4)	82	85.0	1.2 (±0.4)

[a] Assuming a volume of 3×10^{27} cm^3.

[b] For discussion of uncertainties on E, see § IV.

The results of the temperature analysis are given in Table 1. The temperature of regions A–D are all consistent with 3×10^6 K. Using these temperatures in conjunction with the observed fluxes, an emission measure was derived for each location, from which the density was calculated using a volume of 3×10^{27} cm^3. The volume was derived from the area of an FCS pixel and a typical soft X-ray scale height of 3×10^9 cm (for discussion of the scale height in an active region, see Schmahl *et al.* 1982). The assigned uncertainties correspond to the extent of the error box in temperature–emission-measure space based on the statistical uncertainties of the line fluxes (the basic method is discussed by Veck *et al.* 1984). The values of the uncertainties quoted in Table 1 for the temperature and density derived from the X-ray data represent the maximum deviation permitted in each of the parameters that will reproduce the flux in all three X-ray lines to within 1 standard deviation of the observed values.

b) Radio Observations

The radio observations of Hale active regions 16863 and 16864 were made at 6.16 cm with the WSRT during 1980 May 22–27. Approximately 12 hours of observations were used daily to produce full synthesis maps in Stokes parameters I (total intensity) and V (circular polarization) with an E-W resolution of 3.″6–4.″2 and a N-S resolution of 10″–12.″2. The observations have been described in detail by Alissandrakis and Kundu (1982).

Figures 2*a* and 2*b* show the 6 cm total intensity (I) and circular polarization (V) maps for May 25; Figures 3*a* and 3*b* show similar maps for May 26. The reader is referred to the paper by Alissandrakis and Kundu (1982) for overlays of the radio maps with Hα pictures and magnetograms. The ring structure of the 6 cm emission is more prominent in the May 25 I map, in the source associated with the large spot in region 16864, where it shows up as a brightness temperature depression approximately 5×10^5 K, compared with the brightness temperature of the rim which ranges from 1.5×10^6 to 2.5×10^6 K. The radio source associated with the other large spot (region 16863) does not show a clear ring structure. However, the associated 6 cm emission has a broad background with small superposed emission patches with brightness temperatures of up to 3.6×10^6 K.

The circular polarization maps of the sunspot-associated sources, in particular of region 16864 on May 25, shows the characteristic pattern of a ring, i.e., the maximum of V is located at the edge of the total intensity sources. It should be emphasized here that this circular polarization ring is not the same phenomenon as the total intensity ring. The existence of such polarization structures has been pointed out by Alissandrakis, Kundu, and Lantos (1980, see their Fig. 8), while similar structures were more recently observed by Lang and Willson (1982). These polarization rings occur above the penumbra, where only the third and fourth harmonics are located in high-temperature (10^6 K) atmospheric layers; the third harmonic is optically thin in the ordinary mode and optically thick in the extraordinary, which results in high polarization (Alissandrakis 1980; see also § III).

A comparison of the X-ray and radio maps shows that there is little soft X-ray emission associated with the large spots, in particular the spot in region 16864. The X-ray emission peaks around the main neutral lines of the two regions where radio sources also appear (sources C and D); moreover, there is strong Ne IX emission in region E, apparently associated with a radio feature. These structures are discussed in the following sections.

III. RADIO MODELS OF THE RING SOURCE

The X-ray data analysis (Table 1) shows that the electron temperature of the sunspot-associated regions is about the same as the maximum brightness temperature observed at 6 cm; however, the same analysis gives no indication of the presence of low-temperature material above the umbra. In this section, we use model computations of the microwave emission in order to investigate the possibility that the brightness temperature depression observed in the middle of the spot is not due to a lower electron temperature, but rather due to the low-opacity effects.

We note in passing that the computed brightness temperature due to the free-free (f-f) process (Table 1) is considerably lower than the observed temperature, which reconfirms that the gyroresonance (g-r) process is responsible for the sunspot-associated sources of high brightness temperature (Zheleznyakov 1962; Kakinuma and Swarup 1962; Alissandrakis, Kundu, and Lantos 1980).

In this section we present model computations of total intensity and circular polarization (as well as ordinary and extraordinary mode emission) and compare them with the observations. The emission was computed along a line through

the center of the sunspot in the direction of the limb. Both g-r and f-f processes were taken into consideration, although g-r is by far the most dominant (~90% of the emission).

Since the magnetic field measurements at Meudon and Kitt Peak suffered from saturation problems in the spot umbra, we approximated the magnetic field with a vertical dipole, located below the photosphere. The model field parameters were adjusted so that the maximum photospheric magnetic field was 3000 gauss (as measured at Mount Wilson), and the diameter of the 6 cm source was the same as the observed diameter of the ring source. The model field was placed at a heliocentric distance of 20°, since the ring source was at 20°.3 at the midpoint of the observing period on May 25 (E8.7, S19.9) and at 19°.1 on May 26 (W4.4, S19.9). Alissandrakis, Kundu, and Lantos (1980) and Alissandrakis (1980) used the same model for temperature and density, a plane-parallel, constant conductive flux model. In this model, the temperature and density at a height of 2×10^3 km were assumed to be 10^5 K and 5×10^{10} cm^{-3} respectively. Computations were done for a range of values of the conductive flux in order to study the effect of temperature changes; higher conductive flux means higher temperature at a given height.

The results are shown in Figure 4. The total intensity shows a depression, displaced by 7×10^8 cm from the center of the spot in the direction of the disk center, which is due to the angle effect. However, this depression appears only in the ordinary mode emission and not in the extraordinary because, in the latter mode, it is too narrow to show up in the computation. Essentially, the depression corresponds to the region where the angle between the magnetic field and the lines of sight is small enough to make the second harmonic optically thin in the ordinary radiation. Consequently, at the location of the

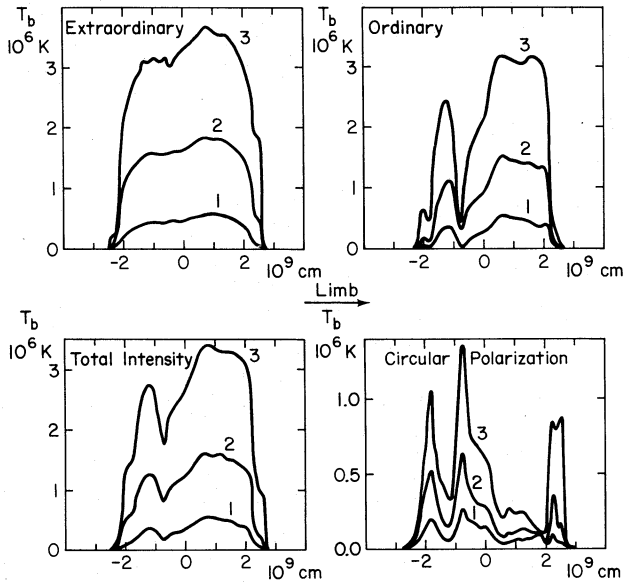

FIG. 4.—Computed brightness temperature at 6 cm along a line through the center of the ring source in the direction of the limb. The computation was done using a vertical dipole field model and a plane-parallel, constant conductive flux model of electron temperature and density, for three values of conductive flux: 3×10^5 cgs units (curve 1), 2.7×10^6 cgs units (curve 2), and 2.47×10^7 cgs units (curve 3). Note the absence of the brightness temperature minimum in the extraordinary mode emission.

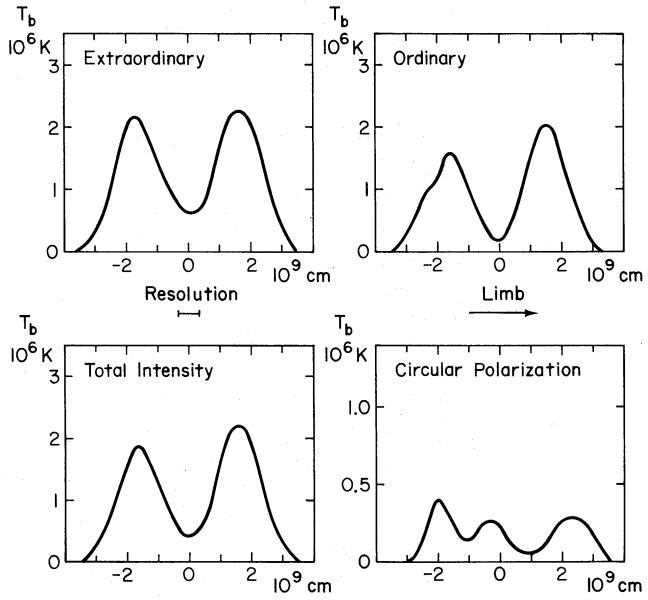

FIG. 5.—Observed brightness temperature along a line through the center of the ring source in the direction of the limb for 1980 May 25 (see Figs. 2*a* and 2*b*). Notice the presence of the brightness temperature minimum in *both* the extraordinary and the ordinary mode emission.

total intensity depression we have a peak in the circular polarization.

We do not discuss here all the features of the plots, but we want to point out the occurrence of two more peaks in the circular polarization plots, located at the edges of the spot and corresponding to the circular polarization rings (see § II*b*). These occur in locations where only the third and fourth harmonics are in high-temperature regions; these harmonics are optically thin in the ordinary mode while they can be optically thick in the extraordinary mode.

We show in Figure 5 plots of the observed *I*, *V*, *e*-mode, and *o*-mode emission through the center of the ring source of 16864 for May 25 (see Figs. 2*a* and 2*b*); as in the case of the model computations, these plots show the variation of the brightness temperature in the direction of the limb. In the comparison of the observations with the models shown in Figure 4, the effects of the instrumental resolution, which is approximately 8″ in the direction of the limb, should be kept in mind; instrumental effects broaden the sources.

The observed circular polarization curve shows three peaks, two at the edges of the spot and one in between, the latter with a small displacement from the center of the source toward the disk center. The general shape is very similar to the model computations, while the middle peak, in particular, indicates that an angle effect is there. However, the minimum of the brightness temperature depression in the total intensity curve does not coincide with a polarization maximum, which, as discussed above, should be the case if the depression were entirely due to the angle effect.

The observed brightness temperature depression is much deeper and wider than that of the models. We also note that the depression shows up both in the extraordinary and the ordinary mode emission, while according to the model it should exist only in the ordinary mode. The near equality of the brightness temperatures in the extraordinary and ordinary

emission modes suggests that the ring structure cannot be interpreted as an opacity difference effect. We can state further that the g-r emitting layers are optically thick for almost the entire extent of the brightness temperature depression and, consequently, that the observed brightness temperature should be about equal to the electron temperature at the level where the radiation is formed. On the basis of this conclusion, there are at least two further possibilities for the interpretation of the ring structures.

1. If, at a given height, the electron temperature above the umbra is the same as that above the penumbra, then the magnetic field above the umbra has to be lower than above the umbra-penumbra boundary. This is necessary so that, above the center of the umbra, the 900 gauss and 600 gauss levels (corresponding to the second and third harmonic of the gyrofrequency) be located at lower regions of smaller electron temperature.

2. At the height of formation of the 6 cm radiation ($\sim$8000 km), there is cool material ($< 5 \times 10^5$ K) above the sunspot umbra and hot ($\sim 2 \times 10^6$ K) material above the pneumbra. This structure is similar to the cool tubes observed by Foukal *et al.* (1974) in the extreme-ultraviolet.

The first possibility is rather hard to accept since it implies that the magnetic field is higher in the penumbra than in the umbra even at the photospheric level. The 6 cm observations would imply a difference in field strength greater than 50%, while the difference at the photosphere could be even larger. However, it is difficult to reconcile the second possibility with the results of the X-ray analysis which show no significant difference in electron temperature or emission measure between the umbra and the pneumbra. These results cannot be attributed to the lower resolution of the XRP; a simple computation on the assumption of a Gaussian shape for the source shows that this effect would increase the observed temperature inside the ring from 0.5×10^6 K to about 0.9×10^6 K; thus the depression would be still observable.

The conclusion that emerges from this analysis is that the hotter plasma that the XRP observed was located at a different height (presumably higher) than the cooler plasma observed by the WSRT. Having no way to establish the absolute height of either emission, we cannot say whether this implies that the height of the 6 cm emission is lower above the umbra or that the X-ray–emitting region is located higher above the umbra than above the penumbra.

IV. SOFT X-RAY FEATURE ASSOCIATED WITH AR 16863

In Figures 1*a* and 1*d*, a compact, bright soft X-ray source (E) is associated with the leading spot in AR 16863. The source is on the edge of the field of view, and, consequently, we cannot observe its full extent in X-rays. Although it is the brightest Ne IX feature on May 25 (Fig. 1*a*), there is no corresponding Mg XI emission (Fig. 1*b*). Ne IX and Mg XI are formed at different temperatures in the corona ($T_{max} = 4 \times 10^6$ K and 7×10^6 K respectively), and hence this feature must be at a lower temperature than the rest of the active region (compared with C or D). From the co-alignment, we find that it is associated with a longlived Hα brightening in the main spot umbra and a corresponding compact microwave source (labeled E in Fig. 2*a*). The microwave source has a brightness temperature of about 3.6×10^6 K.

The soft X-ray source persisted for at least 24 hours, but by May 26 it had decayed to nearly half its original intensity (see Fig. 1*d*), while the 6 cm brightness was almost constant. The XRP also observed it to be bright at 00:24 UT on May 26 (Bentley 1983). It is possible that the decrease in intensity was due to motion of the source with respect to the FCS field of view caused by solar rotation and perspective effects.

Owing to the large degree of overlap between the O VIII, Ne IX, and Mg XI emission functions, we can only estimate the single electron temperature and emission measure that characterize the source. The low Mg XI signal at E established that the temperature must be less than 1.5×10^6 K. It is not possible to derive an accurate temperature from O VIII and Ne IX fluxes as their ratio at low temperatures ($< 3 \times 10^6$ K) is insensitive to temperature variations, as discussed in § II*a*. However, in order to attain the observed fluxes in O VIII and Ne IX at 1.5×10^6 K, a large emission measure is required because both emission functions are dropping steeply from their respective peaks (3×10^6 K and 4×10^6 K respectively). For example, if the temperature were only 1×10^6 K, the emission measure required would be nearly two orders of magnitude greater to reproduce the same fluxes in Ne IX and O VIII. Hence, assuming a temperature of less than 10^6 K would introduce extraordinarily high densities. The emission measure for May 25 is 10^{49} to $10^{50.5}$ cm^{-3} taking temperatures from 1.5 to 1.0×10^6 K respectively. For May 26 the corresponding emission measure values are $10^{48.6}$ to $10^{50.2}$ cm^{-3}. Allowing for the statistical and calibration uncertainties of the X-ray data, we calculate that the count rates in the O VIII, Ne IX, and Mg XI channels of the FCS all would have to deviate from their observed values by between 2 and 3 standard deviations to have a temperature comparable to the rest of the active region (3×10^6 K) or to that of the microwave source (3.6×10^6 K). Hence, it would seem probable that this feature is at a significantly lower temperature and the larger emission measures must apply.

On the basis of its high emission measure, the feature is optically thick to free-free emission (Table 1). However, it is clear that the radio feature cannot be due to free-free emission alone because: (*a*) the observed brightness temperature is about 3 times higher than the value computed on the basis of the isothermal X-ray model; and (*b*) it is located in a region of high magnetic field so that gyroresonance emission alone can account for the observed brightness at 6 cm. Its appearance as a discrete source at 6 cm can be attributed to either a local density enhancement or a local enhancement of the magnetic field, or even to a nonthermal process. However, the magnetogram shows nothing peculiar at the location of the feature; apparently, at 6 cm we observe the upper, hotter part of the dense X-ray feature.

It is clear from the size of the microwave and Hα as well as the X-ray image that this is a compact source. Hence, with such a high emission measure, the density would also have to be large. This coupled with the lower temperature of the feature and its longevity (>24 hours) would require significant energy input to maintain it in its observed state, although this is impossible to quantify given the uncertainties discussed above. However, to our knowledge, this is the first reported observation of a dense, long-lived X-ray feature associated with a sunspot.

V. FEATURES ASSOCIATED WITH X-RAY ARCADES

In this section we discuss two regions of the most intense X-ray emission (C and D in Fig. 1*f*), which are located above the magnetic neutral lines that separate the preceding from the following part of the active regions. From the shape and the position of these features, we conclude that they are arcades of loops, although the 15″ pixel size of the FCS is too large to resolve individual loops. At 6 cm there is strong emission at nearly the same location, with about the same size and shape as the X-ray features (the large sources with peaks marked C and D in Fig. 2*a*). The maximum brightness temperature of peak C is 3.8×10^6 K, while that of D is 3.2×10^6 K. These radio sources are of the type which is sometimes associated with Hα filaments (Kundu *et al.* 1977; Alissandrakis and Kundu 1982).

Using the X-ray and the radio observations, we can draw conclusions about the origin of the radio emission. Let us first note that, within the limits of observation errors, the electron temperatures of regions C and D (computed from the X-ray data) are about the same as their brightness temperatures at 6 cm; consequently, the radio features must be optically thick, assuming that the radiation is thermal. Furthermore, from the electron temperatures and emission measures derived from the X-ray data, we computed the free-free optical depth and the corresponding brightness temperature (Table 1). The brightness temperatures computed in this way are much lower than the observed ones at 6 cm. A more accurate computation can be made by assuming a model for the temperature and density variation with height in the transition region above the neutral line, such as a constant conductive flux model. Expressions for the optical depth and the brightness temperature for such a model have been given by Alissandrakis, Kundu, and Lantos (1980); using these expressions and the parameters derived from the X-ray data, we obtain an upper limit for the free-free brightness temperature 50% higher than the one deduced from the isothermal model, but still too low by a factor of 4–10 to account for the observed microwave emission in terms of the free-free process. (For more details see the appendix.)

These computations imply that the bulk of the radio emission from these sources is not due to the f-f process. The same conclusion was drawn by Schmahl *et al.* (1982), who observed radio emission associated with an X-ray arcade between two spots of opposite polarity.

Further evidence against the f-f origin of this type of 6 cm emission is provided by the high degree of circular polarization (40%–60%). A possible explanation which has not been checked with model computations yet is that the gyroresonance process at harmonics higher than the third may be responsible for the emission (Kundu *et al.* 1977). Emission from nonthermal particles cannot be entirely excluded. We consider it unlikely because of the stability of the sources during the entire observing period of 6 days; however, no computation has been done yet of the number and energy range of particles that could account for the observed brightness temperature and could show whether these particles could be produced under the conditions prevailing near neutral lines. Such computations are beyond the scope of this paper.

VI. SUMMARY AND CONCLUSIONS

The combined observations of two active regions with the WSRT and the XRP have given complementary information on the physical conditions in the low corona and the mechanisms responsible for the 6 cm emission. In this paper we have investigated three kinds of structures, namely, a brightness temperature depression associated with sunspot umbra, an X-ray bright point observed above a sunspot, and an arcade of coronal loops.

The comparison of our model computations of the sun-sunspot-associated ratio emission with the observations show that, although part of the brightness temperature depression inside the ring can be attributed to the low opacity of the g-r layers, the bulk of the depression must be due to the formation of the radio emission in regions of low electron temperature. This implies either that low-temperature material is present above the umbra at coronal heights or that the magnetic field configuration is such that the maximum field intensity occurs in the spot penumbra rather than in the umbra. While it is difficult to accept the latter interpretation, the analysis of the X-ray data does not confirm the presence of low-temperature material. Apparently, the X-ray–emitting plasma is located above the lower temperature plasma that emits the 6 cm radiation.

Strong radio sources ($T_b \sim 3 \times 10^6$ K), associated with neutral lines of the magnetic field, were also associated with what appears to be arcades of coronal loops. Using the electron temperature and emission measures determined from the X-ray data, we conclude that only a small part of the 6 cm emission can be attributed to the free-free process. It appears that the emission, if thermal, is mainly due to the g-r process (Kundu *et al.* 1977; Schmahl *et al.* 1982). The strong polarization of such sources also argues against the f-f process. Model computations are needed to check the possibilities of g-r or nonthermal origin of the emission.

Finally, the X-ray bright point which is more prominent on May 25 appears to be associated with a patch of radio emission. The X-ray data indicate that this is a low electron temperature ($T_e \sim 1.2 \times 10^6$ K), high emission measure ($\sim 10^{49.8}$) structure. This makes it optically thick to f-f emission at 6 cm. However, its observed brightness temperature is about 2 times higher, which means that most of its radio emission is due to the g-r process.

The WSRT is operated by the Netherlands Foundation for Radio Astronomy with financial support from the Netherlands Organization for the Advancement of Pure Research (ZWO). K. T. S. was supported by NASA contract NAS 5-23758 and the Lockheed Independent Research Program. The XRP was built by a consortium of three groups: Lockheed Palo Alto Research Laboratory, Mullard Space Science Laboratory, and the Rutherford and Appleton Laboratories. The latter two groups were supported by the United Kingdom Science and Engineering Research Council. The work of M. R. K. was supported by NSF grant ATM 8103089, NASA grant NGR 21-002-199, and NASA contract NSG 5320. The work of C. E. A. was supported by the University of Athens.

APPENDIX

COMPUTATION OF THE FREE-FREE BRIGHTNESS TEMPERATURE

The analysis of the X-ray data under the assumption that the temperature of the emitting region is constant gives an estimate of the electron temperature and the emission measure. On the basis of this information, one can compute the microwave optical depth and brightness temperature and compare the latter with high-resolution microwave observations. Assuming an isothermal model, the microwave optical depth is

$$\tau = \frac{0.16Y}{f^2 T_e^{3/2}}, \tag{A1}$$

where T_e is the electron temperature, f is the frequency of observation, and $Y = \int n_e^2 dl$ is the emission measure. The brightness temperature of the region is then

$$T_b = T_e[1 - \exp(-\tau)] \approx T_e \tau = \frac{0.16Y}{f^2 T_e^{1/2}}, \tag{A2}$$

where the last two expressions are valid for $\tau \ll 1$.

Estimates obtained in this way are rather crude, since the radiation is actually formed in a region of widely varying temperature (the transition region and low corona) and the low-temperature material will enhance the optical depth. A better estimate can be obtained if one uses a model for the temperature and density variation with height. The simplest such model is one which assumes that the radiation is emitted in a layer with a temperature T_1 at the lower boundary and a temperature T_2 at the upper boundary and that the temperature and density are such that the ratio of the conductive flux to the square of the pressure is constant. Then the brightness temperature of the layer is (Alissandrakis, Kundu, and Lantos 1980):

$$T_b = T_2 \left[1 - \frac{T_1}{T_2} \exp(-\tau)\right] \frac{\Gamma}{\Gamma + 1}, \tag{A3}$$

where $\mathrm{T} = \Gamma \ln (T_2/T_1)$ is the optical depth of the layer; Γ is a constant given by $\Gamma = 0.16p^2 A/(f^2 F_c)$, where $p = n_e T_e$ is proportional to the electron pressure, $A = 1.1 \times 10^{-6}$ cgs units, and F_c is the conductive flux. The emission measure is

$$Y = \int n_e^2 dl = \frac{2}{3} \frac{p^2 A}{F_c} (T_2^{3/2} - T_1^{3/2}). \tag{A4}$$

Thus, in terms of the emission measure, the constant Γ becomes

$$\Gamma = 0.24 Y f^{-2} (T_2^{3/2} - T_1^{3/2})^{-1}. \tag{A5}$$

In our case, T_2 corresponds to a coronal temperature of approximately 3×10^6 K while T_1 corresponds to the base of the chromosphere-corona transition region, so that we can assume $T_2 \gg T_1$; then the expression for the brightness temperature becomes

$$T_b \approx \frac{0.24 Y T_2}{0.24Y + f^2 T_2^{3/2}}. \tag{A6}$$

It is reasonable to assume that an upper limit of T_2 is given by the value of the temperature deduced from the X-ray analysis; this, together with the value of the emission measure deduced again from the X-ray data, gives an upper limit for the free-free brightness temperature in the microwave range. In our case, the optical depth computed under the isothermal approximation is small, and $0.24Y \ll f^2 T^{3/2}$ in equation (A6). Therefore, it is clear from equations (A2) and (A6) that the constant conductive flux model predicts a brightness temperature 50% higher than the isothermal model.

REFERENCES

Acton, L. W., and Brown, W. A. 1978, *Ap. J.*, **225**, 1065.
Acton, L. W., *et al.* 1980, *Solar Phys.*, **65**, 53–71.
Alissandrakis, C. E. 1980, in *IAU Symposium 86, Radio Physics of the Sun*, ed. M. R. Kundu and T. E. Gergely (Dordrecht: Reidel), p. 101.
Alissandrakis, C. E., and Kundu, M. R. 1982, *Ap. J. (Letters)*, **253**, L49.
Alissandrakis, C. E., Kundu, M. R., and Lantos, P. 1980, *Astr. Ap.*, **82**, 30.
Bentley, R. D. 1983, private communication.
Foukal, P. V., Huber, M. C. E., Noyes, R. W., Reeves, F., Schmahl, E. J., Timothy, J. G., Vernazza, J. E., and Withbroe, G. L. 1974, *Ap. J. (Letters)*, **193**, L143.
Kakinuma, T., and Swarup, G. 1962, *Ap. J.*, **136**, 975.
Kundu, M. R., Alissandrakis, C. E. Bregman, J. A., and Hin, A. 1977, *Ap. J.*, **213**, 378.
Kundu, M. R., Schmahl, E. J., and Rao, A. P. 1981, *Astr. Ap.*, **94**, 72.
Kundu, M. R., and Velusamy, T. 1980, *Ap. J. (Letters)*, **240**, L63.
Lang, K. R., and Willson, R. F. 1982, *Ap. J. (Letters)*, **255**, L111.
Schmahl, E. J., Kundu, M. R., Strong, K. T., Bentley, R. D., Smith, J., Jr., and Krall, K. 1982, *Solar Phys.*, **80**, 233.
Veck, N. J., Strong, K. T., Jordan, G., Simnett, G., Cargill, P. J., and Priest, E. 1984, *M.N.R.A.S.*, in press.
Webb, D. F., and Zirin, H. 1981, *Solar Phys.*, **69**, 99.
Zheleznyakov, V. V. 1962, *Astr. Zh.*, **39**, 5 (English transl. in 1962, *Soviet Astr.—AJ*, **6**, 3).

C. E. ALISSANDRAKIS: Laboratory of Astrophysics, University of Athens, Panepistimiopolis, Athens, 621 Greece

M. R. KUNDU: Astronomy Program, University of Maryland, College Park, MD 20742

K. T. STRONG: Space Astronomy Group, Lockheed Missiles and Space Company, 3251 Hanover Street, Palo Alto, CA 94304